Materials and Design 197 (2021) 109200

Contents lists available at ScienceDirect

Materials and Design

journal homepage: www.elsevier.com/locate/matdes

Nanocellulose-enriched hydrocolloid-based hydrogels designed using a Ca^{2+} free strategy based on citric acid

Adriana Lungu [a], Alexandra I. Cernencu [a], Sorina Dinescu [b], Roxana Balahura [b], Paul Mereuta [c], Marieta Costache [b], Kristin Syverud [d,e], Izabela C. Stancu [a,*], Horia Iovu [a,f]

[a] Advanced Polymer Materials Group, University Politehnica of Bucharest, 1-7 Gh. Polizu Street, 011061 Bucharest, Romania
[b] Department of Biochemistry and Molecular Biology, University of Bucharest, 91-95 Splaiul Independentei, 050095 Bucharest, Romania
[c] Horia Hulubei - National Institute for Physics and Nuclear Engineering (IFIN-HH), 30 Reactorului Street, 077125 Magurele, Romania
[d] RISE PFI, Høgskoleringen 6B, NO-7491 Trondheim, Norway
[e] Department of Chemical Engineering, Norwegian University of Science and Technology, Trondheim, Norway
[f] Academy of Romanian Scientists, 54 Splaiul Independentei, 050094 Bucharest, Romania

HIGHLIGHTS

- Fully biomass-based nanostructured hydrogels were obtained by a novel non-conventional physical gelation using citric acid.
- Hydrogels were prepared from vegetable hydrocolloids, namely alginate or pectin, each combined with oxidized nanocellulose.
- Citric acid-crosslinked hydrogels provide more cell-friendly enem environments compared to the calcium-crosslinked counterparts.
- Citric acid-crosslinked hydrogels present higher elasticity compared to calcium-crosslinked ones.

GRAPHICAL ABSTRACT

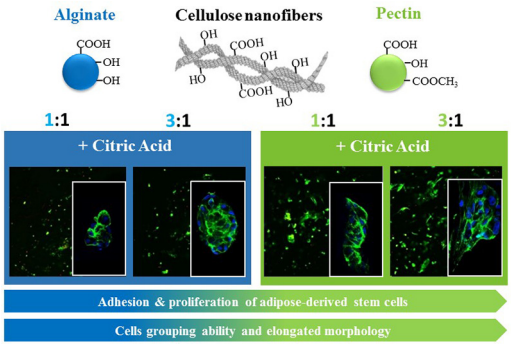

ARTICLE INFO

Article history:
Received 25 June 2020
Received in revised form 24 September 2020
Accepted 28 September 2020
Available online 30 September 2020

Keywords:
Hydrocolloids
Wood-derived nanocellulose
Cellulose nanofibrils
Polysaccharide-based hydrogels
Ca^{2+} free hydrogels
Citric acid-crosslinked hydrogels

ABSTRACT

In this work fully biomass-based hydrogels were developed using a naturally occurring vegetable hydrocolloid co-mingled with wood-derived nanocellulose fibrils. Two distinct types of hydrocolloids have been considered: a seaweed-derived biopolymer (alginate) and a plant-derived biopolymer (pectin). To attain nano-structured binary hydrogels, surface-functionalized cellulose nanofibrils (CNFs) bearing carboxyl groups were employed. This study addresses a non-conventional approach of physical gelation that takes place in acidic conditions (pH < 3) at ambiental temperature using citric acid as gelation-inducing additive in comparison with the typical Ca^{2+}-crosslinked hydrogels. The use of a specific crosslinker directly determines the gross properties of the material because of different type and density of polymer junctions and chains assembly. Therefore, the final features of the bioinspired scaffolds such as moisture uptake, morphological and mechanical characteristics are strongly influenced by the type of gelling additive used and by the ratio between the employed vegetal polysaccharides. Citric acid-based hydrogels presented a higher stability when compared to the calcium-mediated controls and a significantly higher proliferation was detected when raising the hydrocolloid content and when citric acid was used for crosslinking. The newly adopted crosslinking strategy provides a more cell-interactive microenvironment than calcium-based crosslinking leading to improved viability and cytoskeleton development of stem cells.

* Corresponding author.
E-mail address: izabela.stancu@upb.ro (I.C. Stancu).

https://doi.org/10.1016/j.matdes.2020.109200

1. Introduction

Advances in tissue engineering fundamentally relay on combining cells, materials and engineering in a purpose to replace damaged tissues or to improve their functions [1]. To tailor specific solutions to specific problems, a whole range of strategies have been proposed and one of them is represented by designing absorbable polymer scaffolds made of natural compounds with increased biocompatibility that will outturn the cellular response [2]. Although natural polymers are a mature area of research and are already being spun out into clinical applications, the biomedical field still deals with finding one approach that will cope more efficiently with the patient needs.

Exploiting the properties of naturally occurring compounds for biomedical applications has a long tradition and the cascading findings on heteropolysaccharides motivate the study of alginates (ALG) and pectins (PEC) that are found in either marine plants (isolated from brown seaweeds) or land plants (the cell wall of most plants, such as apple and citrus). Due to their low cost, biocompatibility, and renewability, both ALG and PEC are widely used biopolymers in many fields such as drug delivery [3–7], tissue engineering [8–10], and food industry [11,12]. Both types of polysaccharides derive their (strong) anionic character from carboxyl groups of sugar constituents: mannuronic (M) and guluronic (G) acids for ALG and galacturonic acid (partially methylated) residues for PEC. These heteropolysaccharides are considered to be a promising line of research in the tissue engineering field since they show a high potential for mimicking the native extracellular matrix (ECM) on account of the acidic sugars in the polymer backbone akin to glycosaminoglycans (such as hyaluronic acid) [13].

Among plant-derived polysaccharides, wood based nanocelluloses recently came into sight as natural compounds opening an opportunity for the development of a new generation of eco-friendly nanomaterials. The nanocellulose-based materials gained a rapidly growing interest since the nanocellulose fiber diameter is consistent with the width of native ECM fibers (50–500 nm) and on this wise are likely to mimic the physiological environment [14]. In addition to its nanometric dimensions, nanocellulose imparts several fascinating properties such as high strength, excellent stiffness, and high surface area from which the biomedical field can tremendously benefit [15–19]. The advantages of nanocelluloses become all more significant if their surface properties are tweaked through controlled oxidative treatment by introducing -COOH groups on cellulose nanofibrils (CNFs) [20]. This strategy turned out into a key element for successful production of nanocellulosic gels for tissue engineering [21].

With regard to the strong hydrophilic character of polysaccharides, since ALG and PEC are classified as hydrophilic colloids and oxidized CNFs form stable colloidal water dispersions, an efficient crosslinking is needed in order to adjust the network stability and to achieve convenient mechanical properties [22]. One scaffolding strategy for ALG hydrogels that gained popularity in tissue engineering involves gelling by ionotropic crosslinking by the use of Ca^{2+} under mild gelling conditions (physiological pH, ambient temperature) [23–25]. The egg-box model describes the zigzag structure of the junction zones induced by divalent ions that selectively interact with the carboxylate groups on the G residues. However, the main shortcoming of this strategy to achieve stable gels is that in physiological media the ionic exchange with monovalent ions highly affects the polymer crosslinking extent in the way that gel appears to undergo a slow decomposition whereby the excess of Ca^{2+} also rises serious concerns. In contrast to ALG-based hydrogels, PEC- gelling mechanism depends on the degree of methoxylation (DM) based on which PEC is of two types: high methoxyl PEC (HMP) with DM > 50%, and low methoxyl PEC (LMP) with DM < 50% [26]. While HMP forms gels in the presence of sugars at a pH lower than 3.5, where the mechanism is governed by both hydrogen bonds and hydrophobic interactions [27,28], LMP can form hydrogels with divalent cations (such as Ca^{2+}) through ionic crosslinks with non-esterified galacturonic acid units [29]. Due to its structural similarity to ALG, for the gelation mechanism of LMP with Ca^{2+} the "egg-box model" was proposed as well [30]. Moreover, LMP is able to form gels in a wider acidic pH range [31,32].

A non-conventional method for physical gelation of ALG recently regained interest as an alternative strategy to classical divalent metal salts and it could grow into a promising avenue for the biomedical applications of ALG and structurally similar compounds bearing multiple -COOH groups. Pérez-Madrigal and coworkers reported the effectiveness of small organic molecules such as dimethyl sulfoxide or multifunctional carboxylic acids as crosslinker agents for ALG [33]. This paper describes a strategy for room temperature synthesis of hydrogels that is based on the property of ALG to undergo a sol/gel transition process upon lowering the pH below the pKa value of the uronic acid residues as previously reported by Draget and co-workers [34–36] to achieve stable gels.

The use of Ca^{2+} can be a problem in connection with scaffolds for tissue engineering due to its anticoagulant effect through reversible chelation of Ca^{2+} from blood. Thus, we have chosen another approach based on citric acid as naturally occurring low-toxicity crosslinker to obtain Ca^{2+}-free hydrogels. Owing to the valuable pendant carboxyl functionality, citric acid interacts with polymer chains bearing -OH groups leading to ester bond-crosslinks. Such crosslinking reaction usually takes place at high temperatures (>100 °C) eventually in the presence of toxic catalyst (eg. sodium hypophosphite), via a cyclic anhydride intermediate formation. The use of citric acid as crosslinker has been reported in polysaccharide chemistry for the gelation of cellulose derivatives [37–39], starch [40], chitosan [41], ALG [42,43] and PEC [44]. Recently Zheng and coworkers reported a facile approach to fabricate physical crosslinked cellulosic-gels upon the carboxymethyl cellulose acidification in citric acid at ambient temperature [45].

Within the frame of recent findings regarding alternative strategies for physical gelation of polysaccharides (mainly through H bonds), the present work is undertaken to investigate citric acid crosslinking capacity without using heat treatment or any catalyst for the formation of hydrogels derived out of acidic polysaccharides: ALG or LMP combined with CNFs decorated with carboxylic acid functionalities. The citric acid-crosslinked hydrogels properties were investigated compared with their corresponding Ca^{2+}-crosslinked hydrogels. To the best of our knowledge, no prior studies have explored the employment of this strategy to obtain hydrogels that will be more cell-friendly and thus better suited in tissue engineering. The hydrocolloid type as well as the ratio between the combined polysaccharides used in the synthesis process, induce significant structural modifications in hydrogels which latterly influence the performance of hydrogels in terms of swelling and mechanical properties.

In this paper we propose an alternative strategy to design physically crosslinked hydrogels engineered using a naturally derived, cost-effective citric acid aiming Ca^{2+} free ALG or PEC hydrogels for biomedical applications. Considering the green preparation conditions, these nano-cellulosic hydrogels become highly promising platforms for tissue engineering to serve as material-analogues for soft tissue repair or as carriers for drugs or other biomolecules.

2. Experimental section

2.1. Materials

Never-dried bleached-kraft pulp from softwood was kindly provided by StoraEnso™ and used as such for the oxidation treatment. Commercially available alginic acid sodium salt (ALG) from brown algae (low viscosity) with a viscosity of 4–12 cP (for 1% solution in H_2O, at 25 °C) (data were provided by the manufacturer) as well as high-methoxylated pectin (HMP) extracted from apple with an esterification degree of 70–75% were purchased from Sigma-Aldrich.

The reagents used for the chemical modification of cellulose and HMP respectively, such as TEMPO (2,2,6,6-Tetramethyl-1-piperidinyloxy, free radical, 98%), Sodium bromide ACS (≥99%), Sodium hypochlorite solution (NaClO) (12% active chlorine) EMPLURA®, Sodium hydroxide 98% (pellets) and hydrochloric acid ACS (37%) were reagent-grade chemicals purchased from Sigma-Aldrich.

Calcium chloride ≥97.0% (anhydrous, free flowing, Redi-Dri™) was also acquired from Sigma-Aldrich. Citric acid, 99 + % was purchased from Alfa Aesar™. All the reagents were used as received without any purification.

Dulbecco's Modified Eagle's Medium (DMEM) medium, antibiotics solution, phosphate buffered saline (PBS) powder, MTT assay kit for quantitative evaluation of viability, Tox7-KT LDH assay kit for evaluation of cytotoxicity, bovine serum albumine (BSA), Triton-X100, paraformaldehyde (PFA) solution, phalloidin-FITC and Hoechst 33258 solution for fluorescence staining of actin filaments and nuclei were purchased from Sigma-Aldrich, Germany. Fetal bovine serum (FBS) and LiveDead assay kit were purchased from Thermo Fisher Scientific, US.

3. Methods

3.1. Preparation of CNFs

CNF suspension was obtained from never-dried cellulose pulp using the TEMPO/NaBr/NaClO oxidation system described by Saito and coworkers [46]. Briefly, a suspension of 1% cellulose was obtained in 100 mL water containing TEMPO (0.0125 g) and NaBr (0.125 g) and the oxidation reaction was conducted by the addition of NaClO (2.5 mmol) at room temperature under gentle agitation. After 1.5 h of maintaining the pH at 10.5 by adding 0.5 M NaOH, the pH was adjusted to 7 using 0.5 M HCl. The product was thoroughly washed with water and subsequently subjected to homogenization obtaining thus a gel-like suspension of 1.13% (*w*/*v*) solid content. The as prepared TEMPO-oxidized cellulose had a total acidic content of 835 μmol/g determined by conductometric titration (SCAN 65:02 method) suggesting that a considerable percentage of primary hydroxyl groups were converted thought oxidation.

3.2. Preparation of LMP

LMP was prepared according to our previous report [47]. In brief, HMP was chemically modified using the alkaline saponification method at pH 11. The LMP solution was then dialyzed for 2 days and lyophilized obtaining dried pectin. The degree of methylesterification value of LMP was estimated to be about 20% following the procedures described by [48–50].

3.3. Preparation of CNFs-based hydrogels

Several polymeric precursors were prepared by dissolution of either ALG or LMP within CNF gels. Out of each combination of polysaccharides, two precursor mixtures were obtained by varying the mass ratio between the two. Thus, the amount of ALG as well as LMP added with respect to CNFs was of 1:1 and 3:1, respectively. Homogeneous precursor dispersions were obtained under vigorous stirring at room temperature for 15 min. The amount of each formulation was halved and poured in two petri dishes, envisioning two different crosslinking methods. To ensure an efficient crosslinking process and to allow a fast and uniform diffusion of the crosslinker, the polymeric precursors were first frozen at -80 °C and freeze-dried for 48 h. After this, the specimens were immersed for 30 min into the crosslinking solutions: 0.5 M citric acid or 3 wt% $CaCl_2$. To ensure that no residual crosslinking agent remained, the obtained hydrogels were thoroughly washed with distilled water (up to neutral pH in the case citric acid) and freeze-dried for 48 h to obtain the crosslinked polysaccharide sponges. The composition of the hydrogels are summarized in Table 1.

4. Characterization methods

4.1. Gel Content (GC)

The crosslinking efficiency was evaluated by gel content analysis in deionized water (DI) and in PBS. Hydrogel specimens were prepared in triplicate from each composition and their initial dried weight (W_i) was measured. Then, to remove uncrosslinked polymer chains, the samples were immersed in the testing media, at room temperature for 48 h and dried at 40 °C for 48 h until they reached a constant weight (W_f).

Gel content (GC) was calculated using Eq. (1) [51]:

$$GC = \frac{W_f}{W_i} \times 100 \quad (1)$$

4.2. Fourier transform infrared (FTIR) spectrometry

Materials structural features were primarily evaluated by Fourier Transform Infrared (FTIR) measurements using a Vertex 70 Bruker FTIR spectrometer equipped with an attenuated total reflectance (ATR) cell with Ge crystal. In all cases, the FTIR spectra recorded at room temperature using 32 scans in wavelengths ranging from 600 to 4000 cm^{-1}, 4 cm^{-1} resolution.

4.3. Scanning electron microscopy (SEM)

The samples morphology was assessed by using a SEM equipment produced by Zeiss, model EVO MA15 with the following technical characteristics: resolution of 3 nm at an accelerating voltage of 30 kV (in high vacuum, for secondary electrons - SE) and a field of view of 6 mm in diameter at a working distance (WD) of 8.5 mm. The SEM is able to run in high vacuum mode (HV) and variable pressure mode (VP), with the pressure ranging from 10 to 400 Pa.

For the samples the accelerating voltage was 20 kV and the magnification range was 150-500× at a working distance in the range 9–12 mm. The images were obtained using the SE detector in high vacuum and for some samples the variable pressure mode (VPSE) was employed at a very low pressure (20 Pa). Prior to observations, a fine layer of gold was sputtered onto the specimen surface using a bench top evaporator in vacuum (Quorum Technologies) to make the samples become more electrically conductive and avoid surface overcharging.

Table 1
Composition of the CNFs-based nanocomposite hydrogels.

	Polymer composition/100 g			Sample code	
Mass ratio	ALG	LMP	CNFs	citric acid crosslinking	calcium-mediated crosslinking
1:1	1.13	–	1.13	AC11/ci	AC11/Ca^{2+}
	–	1.13	1.13	PC11/ci	PC11/Ca^{2+}
3:1	3.39	–	1.13	AC31/ci	AC31/Ca^{2+}
	–	3.39	1.13	PC31/ci	PC31/Ca^{2+}

4.4. Swelling ratio

The freeze-dried samples were accurately weighed (W_d) and then individually incubated in DI and physiological PBS at room temperature. The wet weight (W_s) of the scaffolds was measured by taking out the soaked materials at predefined time intervals and blotting with a filter paper to remove the surface adsorbed water followed by immediately weighing the samples. The equilibrium value is reached after about 2 h of immersion and the maximum swelling degree (MSD) was calculated using the eq. (2):

$$MSD = \frac{w_s - w_d}{w_d} \times 100 \quad (2)$$

The experiments were performed in triplicate under the same conditions and the average values were reported.

4.5. Elasticity assessment through uniaxial compression tests

The compression tests were performed using a CT3 texture analyzer (Brookfield) equipped with a 4500 g cell and a TA4/100 compression accessory. The synthesized compositions were poured in PDMS molds with a diameter of 5 mm and a height of 3 mm and crosslinked using $CaCl_2$ and citric acid, respectively. The so-obtained samples were placed on the lower plate of the equipment and tested at room temperature up to a strain of 100% at a compression rate of 0.5 mm/s. In order to obtain relevant results, three specimens of each composition were compressed, and a compressive stress-strain diagram was plotted. The values of Young's modulus were calculated from the slope of the linear part of the compression curve, at 2% strain.

4.6. Cell culture model

Human adipose-derived stem cells (hASCs) were isolated from lipoaspirates, after obtaining patient informed consent and in compliance with the regulations in Helsinki Declaration. The cells were cultured in DMEM media supplemented with 10% FBS and 1% antibiotic antimycotic solution and grown at 37 °C in humidified atmosphere. The cells culture was propagated for four passages until the required number of cells for seeding was achieved and regularly observed with a phase contrast microscope.

4.7. Achievement of 3D cultures

Materials were sterilized by exposure to UV light, swollen at equilibrium using culture medium and cut in pieces with diameter of 1 cm^2. hASCs cells were trypsinized, counted and seeded on materials at 2×10^5 cells/cm^2 density through cells suspension distributed over the composites, allowed to adhere and incubated in standard cultures conditions (37 °C, 5% CO_2, humidity) until the assays were performed.

4.8. Biocompatibility assays

To evaluate the biocompatibility of the 3D systems, viability determination and cytotoxicity assays were performed at two and seven days after cells seeding. Cell viability and proliferation profile were quantitatively determined by MTT assay and also qualitatively via the Live-Dead test, while the cytotoxicity of the material was assessed by the LDH assay.

4.9. Live/Dead fluorescence microscopy assay

The Live/Dead assay was performed using a kit containing two dyes, calcein AM and ethidium homodimer (EthD-1), which allowed simultaneous determination of live cells due to a green fluorescence emitted at calcein AM contact with intracellular enzymes and dead cells through a red fluorescence emitted when EthD-1 binds to the nucleic acids.

The Live/Dead assay was performed at two and seven days after cells seeding in materials with optimal dye concentration. The 3D systems were incubated with the staining solution for one hour in the dark and after that the viability was qualitatively determined employing confocal microscopy. The images were captured employing a LSM710 confocal microscope from Zeiss and processed by its corresponding Zen software.

4.10. Cell viability and proliferation- MTT assay

The viability was quantitatively evaluated using a colorimetric method, respectively spectrophotometric MTT (3-(4,5-dimethylthiazolyl-2)-2,5-diphenyltetrazolium bromide) assay at two and seven days after seeding. The 3D systems were incubated with 1 mg/mL MTT for four hours, allowing the reduction of (MTT) to formazan crystals by living cells due to presence of mitochondrial dehydrogenases. The crystals were solubilized using isopropanol and spectrophotometrically measured at 550 nm employing a Flex Station 3 (Molecular Devices, USA). The number of living cells is direct proportional with the concentration of formazan solution obtained.

4.11. Materials cytotoxicity- LDH assay

The cytotoxicity of the proposed materials was evaluated using Tox7-KT Kit based on colorimetric detection of lactate dehydrogenase (LDH) a cytosolic enzyme, released from damaged cells into culture medium. The LDH Assay Kit contained three reagents in equal proportions which allowed the enzymatic reaction between LDH and lactate with generation of pyruvate and reduction of NAD^+ to NADH, following the reduction of tetrazolium salt in red formazan. The culture medium was collected from the 3D systems and mixed with the components of the kit according to the manufacturer's instructions. After incubation at dark and at room temperature for 15 min, the red formazan obtained which is related to LDH activity was spectrophotometrically detected at 490 nm employing (Molecular Devices, USA). The quantity of LDH is direct proportional with the number of damaged cells.

4.12. Cytoskeleton staining

For actin filaments staining, the 3D systems were washed with PBS and fixed with 4% PFA for one hour. After the PFA was removed, the samples were permeabilized with a solution containing 2% BSA and 0.1% triton X-100 for one hour. F-actin filaments were stained using FITC-phalloidin according to manufacturer's instructions and incubation overnight at 4 °C. Hoechst 33342 was used for nuclei staining. The images were captured employing a LSM710 confocal microscope from Zeiss and processed by its corresponding Zen software.

4.13. Statistical analysis

The gel content, swelling ratio, compression and biocompatibility experiments were performed in triplicate ($n = 3$) and the results were expressed as ± standard deviation (SD). Statistical analysis of the data was performed using GraphPad Prism software, one-way ANOVA method and Bonferroni algorithm. Values were considered significant for $p < 0.05$.

5. Results and discussion

In the present study, we considered designing novel hydrogels entirely relied on plant sources by exploring green and cell-friendly methods. Therefore, polysaccharide-based hydrogels (CNFs dispersed within ALG / LMP matrix) are prepared herein using H-bonds crosslinking. This approach involves tuning the ionization state of

functional groups (-COOH), by protonation in an acid environment leading to the formation of H- bonds and gelation. There is a clear advantage in following a method where neither catalyst nor high temperature is needed for the cross-linking process, considering that these factors may be responsible for possible changes of the polymer nature. Ionotropic gelation with $CaCl_2$ is widely used to produce ALG [52] or LMP-based hydrogels [53] and therefore we used this conventional strategy to fabricate control scaffolds for comparison. To better understand behaviour of the new materials, Fig. 1 displays the main interactions occurring when citric acid crosslinked hydrogels are obtained in acidic conditions, while Ca^{2+}-crosslinked hydrogels synthesized at physiological pH are also represented as control. In the systems the reactions are (i) through H-bonds when citric acid is used and (ii) through calcium-gelation when $CaCl_2$ is used. The crosslinking occurs homogeneously between soluble macromolecules (ALG-ALG and LMP-LMP) and heterogeneously at the interface between the nanofibrils and the soluble polymers (CNF-ALG and CNF-LMP). Their density will depend on the composition of each precursor. It is expected that the density of homogeneous intermolecular ALG-ALG or LMP-LMP interactions increases with increasing the amount of soluble polymer in the precursor composite suspensions.

Only few studies have focused on investigating such physical interactions between biopolymer chains [54,55]. Takigami et al. reported H-bonded carboxymethyl cellulose hydrogel formed by dispersing

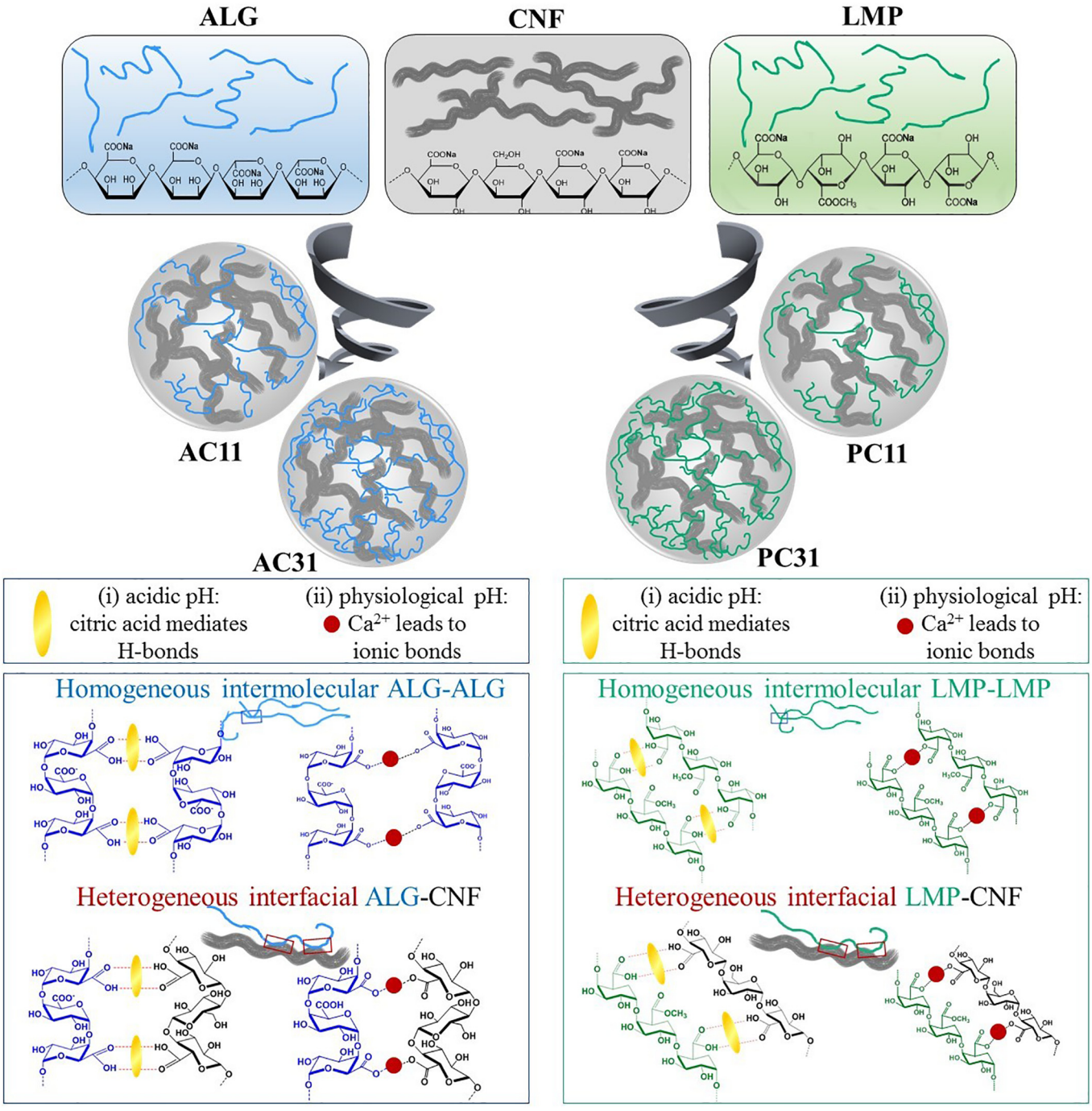

Fig. 1. Schematic representation of the interactions occurring between the components of the AC and PC composite hydrogels using citric acid as crosslinker; comparison with control Ca-mediated crosslinking.

CMC in a HCl solution [56] and similar hydrogels of carboxymethylated-chitosan were obtained in the presence of acids or polyfunctional monomers by Wang et al. [57]. In another work Sandeep and co-workers report hydrogel formed by intermolecular H-bonding between xanthan and alginate [58]. On these grounds, we explored the efficiency of this new crosslinking system for acidic polyssaccharides to achieve stable Ca^{2+}-free nanocomposite hydrogels for tissue engineering.

5.1. Evaluation of materials' gel content

The process of crosslinking implies an increase of interconnected chains on the detriment of solubility leading to the formation of a network that, to one extent, still include unbound polymer chains. In particular, in physically crosslinked hydrogels the interactions between polymer chains prevent dissolution and yet, upon changes in the physical conditions, these interactions can become reversible [51]. Therein, determination of the polysaccharide-based gel content offers a valuable insight on the degree of crosslinking.

Since the formation of the physical hydrogels is entirely based on non-covalent interactions between the macromolecules (ionic, H bonds), investigation of the structural integrity of the crosslinked scaffolds in aqueous conditions is compulsory for the envisaged application of hydrogels in tissue engineering.

The structural stability of citric and control Ca^{2+}-crosslinked hydrogels was assessed in terms of GC% in two different media: deionized water (DI) and physiological buffer (PBS) (both at neutral pH of 7.4) and the results are summarized in Fig. 2.

According to the gel fraction analysis (GC values in Fig. 2), citric acid-based hydrogels presented a higher stability when compared to the calcium-mediated controls, both in DI and PBS. With respect to the determined GC% values, citric acid seems to be an efficient crosslinker for the physical gelation since the H-bonded gels exhibited the highest stability regardless of the immersion media. Gel fraction rises with increasing the amount of ALG or LMP since the yield in the hydrogel formation is dependent on the total polymer concentration. More robust hydrogels seem to be generated using citric acid than with the control method. Such behaviour was expected since the density of intermolecular ALG-ALG or LMP-LMP bonds increases with higher amount of soluble polymer in the precursor. Furthermore, H bonds are generated between a higher number of functional groups per structural unit while calcium salts can only be formed between one group from each structural unit involved. Accordingly, denser networks are expected to be formed through citric acid mediated mechanism. The experimental data confirm the prediction. The highest GC% values were achieved for AC31/ci at 76 ± 3% and for PC31/ci at 79 ± 2%. In contrast, a certain degree of disintegration was observed for all the Ca^{2+}-crosslinked networks since much lower values of GC% were determined. The gel stability explored in DI suggests a minimum GC value of 55% for 11/Ca^{2+} samples and up to 65% for 31/Ca^{2+} samples. When gel stability was assessed in PBS, contents of insoluble part not greater than 35% were obtained for 11/Ca^{2+} samples. These results suggest that, in addition to the solubilized uncrosslinked chains, a degradation through ionic exchange between the Ca^{2+} ions in the egg-box structure and Na^{+} ions present in the buffer takes place, making the network structure loose. Increasing the hydrocolloidal content from 1:1 to 3:1 the more efficient the Ca-mediated cross-linking is, reaching a GC value of about 55%.

The type of hydrocolloid employed revealed minor differences with respect to the amounts of the insoluble part within the polymeric systems, LMP-based materials being slightly more stable.

Overall, it can be noticed that the stability of the samples increases with the increase of ALG or LMP hydrocolloid content, for the two types of crosslinking treatments under investigation. Moreover, using citric acid lead to more stable gels when compared to calcium-treated ones.

5.2. Fourier transform infrared (FTIR) spectrometry

Material structural characterization was performed through FTIR spectrometry by analyzing the characteristic signals of functional groups present in the constituent organic compounds before and after the physical-crosslinking process. In Fig. 3 the characteristic FTIR absorption bands of ALG, LMP, CNFs and citric acid as starting materials (a) and the spectra of crosslinked nanocomposite hydrogels (b) are illustrated.

Several hydroxyls and one carboxyl group are the key functionalities of the three carbohydrate polymers employed in the present study providing support to the formation of hydrogel molecular assemblies. Since all the used polysacharides were employed in the form of Na-type, an intense signal associated with C═O asymmetric stretching vibration of sodium carboxylate groups can be observed in between 1600 and 1630 cm^{-1} (1603 cm^{-1} for Na-ALG and LMP, 1621 cm^{-1} for CNFs – indicated as orange arrow in Fig. 3) while the band assigned to the symmetrical deformation of the COO^{-} groups appears at about 1414 cm^{-1} (black arrow) for all the neat polymers [49,59]. The structural resemblence of the citric acid crosslinking agent with the polymeric substrate makes a straightforward spectral interpretation of FTIR difficult.

The FTIR data of citric acid-crosslinked hydrogels in comparison with the spectra of Ca^{2+}-crosslinked hydrogels revealed differences considering the major absorption bands such as O—H stretching and C═O

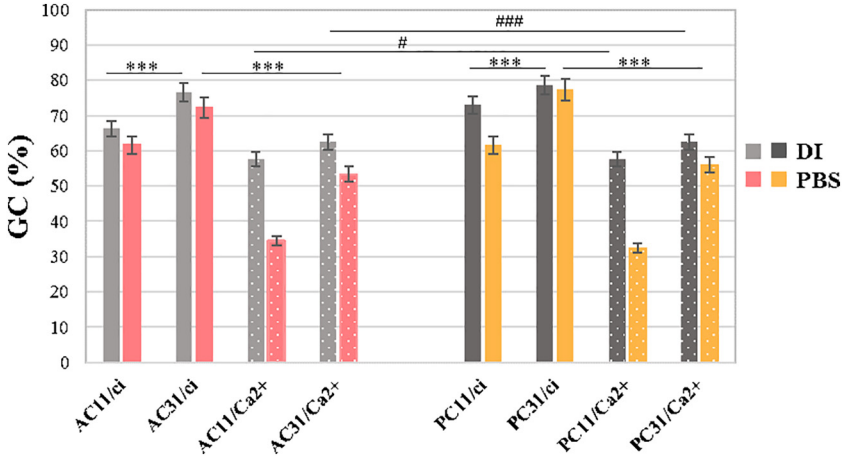

Fig. 2. Influence of the synthesis method on the gel content (GC %) of polysaccharide-based hydrogels determined in DI and PBS: ***$p < 0.001$ (AC11/ci versus AC31/ci in DI, AC31/ci versus AC31/Ca^{2+} in PBS, PC11/ci versus PC31/ci in DI, PC31/ci versus PC31/Ca^{2+} in PBS), #$p < 0.05$ (AC11/Ca^{2+} versus PC11/Ca^{2+}in DI), ###$p < 0.001$ (AC31/Ca^{2+} versus PC31/Ca^{2+}in DI).

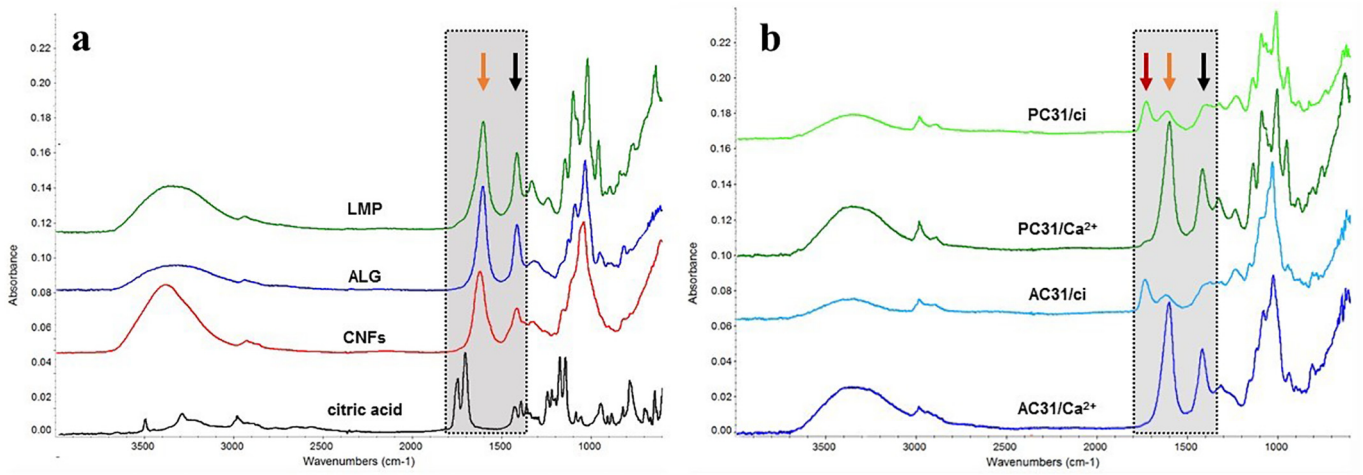

Fig. 3. FTIR comparative spectra of a) neat materials; b) citric acid or Ca^{2+} crosslinked hydrogels.

stretching bands after the interaction with citric acid. The decreasing in intensity and broadening of OH vibration band (3000–3600 cm^{-1}) could indicate H bonding considering the existence of multiple OH functional groups in carbohydrate components structures. Nevertheless, the carboxylate characteristic signal yet appears at around 1600 cm^{-1}, suggesting that some -COONa still exist in the hydrogels after the acidification process. The most important feature is the presence of the signal at 1730 cm^{-1} which is an indication that most of the -COOH are protonated (indicated as red arrow in Fig. 3). The FTIR data demonstrate that the polymer chains carry two kinds of groups: -COONa and -COOH. While the sodium carboxyl groups can form intra- or inter- hydrogen bonds only with alcoholic hydroxyl groups, free -COOH can form intra- or inter- hydrogen bonds with hydroxyl groups or other carboxyl groups generating a crosslinked network [45,60].

Since the complex system of polysaccharides comprises mostly polyuronic acids in their salt form (Na-type), at neutral pH there is a strong electrostatic repulsion which increases the intermolecular distance. Therefore, it seems reasonable to assume that when -COO- groups are protonated, the electrostatic repulsion is diminished favoring the formation of inter-molecular H bonding interactions and, as a result, of physical gels.

From calcium-mediated hydrogels spectra (Fig. 3b FTIR spectra of AC31/Ca^{2+}; PC31/Ca^{2+}) it can be observed that the peak assigned to the symmetrical deformation of the COO^- groups exhibit a displacement towards higher wavelengths as the corresponding signal is recorded at 1427 $\pm$ 2 cm^{-1} when ALG or LMP are respectively used as matrix to disperse CNFs. This shifting was expected and provides an evidence of the ionic crosslinking of the carboxylate groups present in the system since calcium metal ions replaced sodium ions [59,61]. Moreover, the absorption signal of stretching vibrations of O—H bonds in Ca^{2+}-crosslinked samples seems to be narrower compared with the one recorded for the raw materials probably due to the formation of chelating structure in which the effect of hydrogen bonding is reduced [62].

5.3. Scanning electron microscopy (SEM)

The porous microarchitecture of the hydrogels was investigated by SEM. Fig. 4 is representative in this respect.

The SEM micrographs of nanocomposite scaffolds showed porous scaffolds, with architectures strongly depending on the composition of the hydrogels and on the crosslinking method, as visible in Fig. 4. CNFs appear to be well-integrated with either ALG or LMP since no phase separation is noticed. The distinct structuring mainly relies on the crosslinking strategy due to the different interaction patterns occurring between ALG / LMP and CNFs. The way of structure stabilization via citric acid or Ca^{2+} gelation turned out to be one of the key parameters that strongly influence the morphology and network density.

Micrographs of citric-crosslinked scaffolds revealed a highly porous morphology. The development of homogeneously distributed dendritic pores was noticed for all compositions that underwent acidification treatment, indicating that the crosslinking strategy is the main determinant of the microstructuring of the final dried products. Moreover, citric acid is believed to inhibit ice crystallization [63] and strong hydrogen bonding is also considered a factor that may prevent ice crystal growth [64]. Accordingly, it can be concluded that the acidification treatment stimulates the formation of denser small crystals later leading to more numerous pores within the scaffolds.

In addition, it can be observed that pore formation is affected by the increase of solid fraction in the scaffold as well as by the type of heteropolysaccharide used. In particular, AC11/ci developed larger voids (50-100 μm) in comparison with AC31/ci (30-60 μm) and similarly, PC11/ci (20-40 μm) in comparison with PC31/ci (15-30 μm). Higher ALG or LMP concentration decreases the size of the pores. Smaller dendrites are developed as a consequence of higher viscosity that hinders the ice crystal growth during freezing.

The morphological evaluation of the ionic nanocomposites revealed a significant difference in the morphology of the polymeric structuring since, in comparison with citric-crosslinked samples, Ca^{2+}- crosslinked blends gave rise to internal laminar structuring with separated by generous interlayer spaces. Apart from the foliated appearance of scaffolds, it can be observed that the thickness of the plies increases with the amount of heteropolysaccharide present in the blend (15 $\pm$ 4 μm for AC11/Ca^{2+} and 24 $\pm$ 8 μm for AC31/Ca^{2+}; 10 $\pm$ 6 μm for PC11/Ca^{2+} and 22 $\pm$ 5 μm for PC31/Ca^{2+}).

Moreover, it is of value to notice that the addition of a specific hydrocolloid within CNFs suspension plays an essential role upon the formation of porous fibrous structure. LMP-based scaffolds exhibited a more delicate aspect of the network structure with thinner walls (when the crosslinking is mediated by Ca^{2+}) or smaller pores (when the crosslinked in citric acid solution) in comparison with ALG-blends.

The morphological characteristics of the materials are expected to have a primary effect on the swelling properties since the water diffusion process is favored within a homogeneous internal porosity, whereas interlayer porosity is shown to accommodate smaller proportions of water. With regard to the porosity of the obtained scaffolds, the large distribution of pores is in line with the required porosity for a cell attachment and growth, and efficient diffusion and transfer of nutrients/ oxygen within scaffolds.

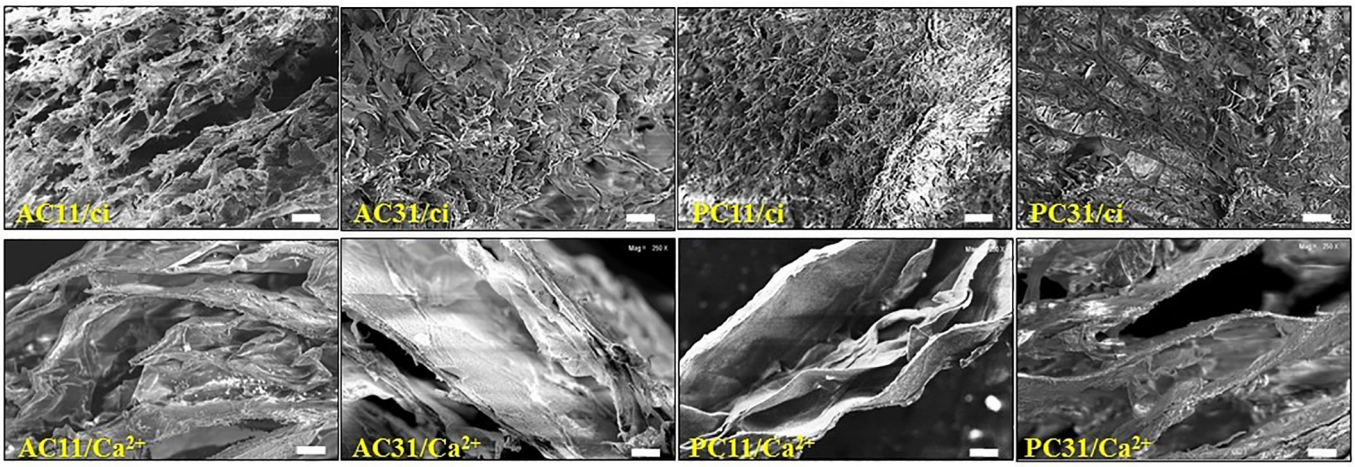

Fig. 4. Influence of the composition and crosslinking method on the porosity of the freeze-dried hydrogels as revealed by representative SEM micrographs (cross-sections) – scale bar 100 μm.

5.4. Determination of the Moisture Uptake of the Gels

The hydrophilic character and swelling properties of the hydrogels with different gelation mechanism were evaluated after 24 h of incubation as maximum swelling degree (%MSD) in Fig. 5, in two different media: deionized water (DI) and physiological buffer (PBS) (both at neutral pH of 7.4).

ALG as well as LMP are colloidal substances with a high affinity for water, a distinguishing feature that highly impact the swelling behaviour of the systems. Besides, CNFs enable an important capacity to bind substantial amounts of water. According to Fig. 5, a relationship between gelation mechanism and the degree of swelling in aqueous media under neutral conditions could be defined. The degree of swelling is significant at a pH higher than the pKa of the polymers since the uronic acid containing polysaccharides are bearing a large number of ionisable functional groups (in particular - COO-) that grant the hydrophilic character.

Foremost, it can be observed that in both DI and PBS, the fluid uptake capacity proved to be largely affected by the gelation mechanism: higher swelling is achieved by citric crosslinked networks in contrast with the samples crosslinked by Ca^{2+}.

Citric-crosslinked hydrogels present pronounced swelling behaviour inherited from the nature of H bonds linkages which would readily interact with water. The swelling capacity of the hydrogels formed by interaction with citric acid revealed no substantial differences in neither DI nor PBS but instead, the obtained data pinpoint a significant increase of the MSD (values in the range of 1200–1700%). Herein, the hydrogel network undergoes a conversion of COOH to COO^- in aqueous media and thus, breaking the hydrogen bonding led to a high swelling extent [65]. The formation of H-bond interactions is advantaged at higher polymer concentration, leading to compact network structuring which in consequence hinder the swelling process. Thus, the MSD value of heteropolysaccharide rich samples decreases with increasing the amount of ALG or LMP. With regard to the morphological effect on swelling behaviour of hydrogel is worthy to notice that in spite of common features like high homogeneity and porosity of the microarchitecture, a dimensionally reduced porosity appears to impede the swellability.

The egg-box model that describes the calcium crosslinked pattern of the control hydrogels seems to be more restrictive in terms of chain expansion. The lowest MSD values were determined in DI, in the range of 200–600% and 300–700% for ALG and LMP-based hydrogels respectively. Nonetheless, swelling tests in PBS provided a higher MSD validating the idea that ion-exchange promotes an additional relaxation of the network and thus enhances the swelling [66]. Moreover, the morphological features of the samples impact the water infiltration. Hence the

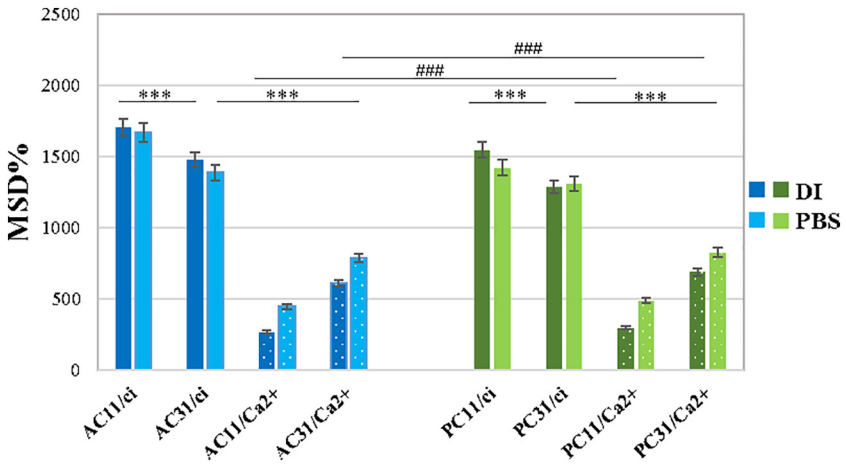

Fig. 5. Influence of the composition on the swelling ratio of the synthesized hydrogels.: ***$p < 0.001$ (AC11/ci versus AC31/ci in DI, AC31/ci versus AC31/Ca^{2+} in PBS, PC11/ci versus PC31/ci in DI, PC31/ci versus PC31/Ca^{2+} in PBS), ###p < 0.001 (AC11/Ca^{2+} versus PC11/Ca^{2+} in DI, AC31/Ca^{2+} versus PC31/Ca^{2+} in DI).

Ca^{2+}-crosslinked samples exhibit large interlayer voids, thick walls are expected to reduce the water permeability. Whereas the swelling of Ca^{2+} gels is dependent on the external environment, the fluid absorption is also liable on the amount of hydrocolloid. Our data also suggest that the polymer ratio turned in favor of heteropolysaccharide increase the hydrophilic character of the ionotropic bi-component systems.

5.5. Elasticity assessment through uniaxial compression tests

The mechanical response of the hydrogels was experimentally investigated through uniaxial compression experiments. The results showed that the type of carbohydrates as well as the ratio between the biopolymers has a strong influence over the materials elasticity. The stress-strain profiles are shown in Fig. 6 and they indicate that all hydrogels present a linear elastic behaviour, followed, at higher strains, by plastic deformations. Two factors, namely the ratio between the matrix components and the crosslinking strategy seem to influence the elastic regime of each binary hydrogel. It can be noticed that for 1:1 samples, citric acid-crosslinked material present a shorter elastic region when compared to their Ca^{2+}-crosslinked counterpart, for both ALG and LMP-based series. For example, AC11/ci is linearly compressed up to about 52% strain, while AC11/Ca^{2+} is elastically compressed up to approximately 75% strain. PC11/ci deforms elastically up to 70% strain, while PC11/Ca^{2+} up to around 77% strain. Increasing the hydrocolloid content from 1:1 to 3:1 extends the elastic deformation domain of citric acid-crosslinked hydrogels as visible in Fig. 6. In contrast, Ca^{2+} crosslinking shortened the elastic deformation interval at higher ALG or LMP content. Another interesting effect of citric acid expressed in samples with the highest hydrocolloid amount (3,1) is the extension of the strain interval specific to the elastic deformation. This behaviour can be correlated with the hydrophilic character previously reported.

In the elastic deformation region, it can be observed that the citric acid-crosslinked hydrogels present higher elasticity compared to Ca^{2+}-based hydrogels (insets in Fig. 6). When crosslinked with citric acid, similar Young's modulus values were determined for both ALG and LMP-based hydrogels, the resemblance in elasticity indicating that the mechanical features are not reliant on the type of hydrocolloid used. Nonetheless it can be observed that, when crosslinked with calcium, ALG-based hydrogels show higher Young's modulus in comparison with LMP-based materials, the ionic networks generated by galacturonic units of pectin exhibiting higher elasticity. Despite the crosslinking method, ALG- and LMP-richer hydrogels exhibit a higher Young's modulus in comparison with the hydrogels containing equivalent polymer compositions since the addition of higher amounts of carboxylate-rich compound (ALG / LMP) within the polymeric matrix will increase the number of crosslinks.

5.6. Cell viability and proliferation- MTT assay

Considering the novel crosslinking strategy, the evaluation of cellular response to the nanocomposite hydrogels was fundamentally required. The rate of viability and proliferation of hASCs in the porous scaffolds was evaluated by MTT assay after two and seven days post-seeding.

The results revealed a good biocompatibility of the assessed materials in contact with hASCs indicating that the combination between CNFs and ALG or LMP is favourable for cell growth (Fig. 7 a, b). The assessment of cell viability revealed appealing results for citric-crosslinking method since a slight tendency of increased viability was observed for cells grown in AC/ci, as compared to AC/Ca^{2+} and an even more pronounced viability rate in PC/ci, as compared to PC/Ca^{2+}.

Examining ALG-based scaffolds after two days of culture with respect to the ratio between the two polymers, minor differences were observed in cellular viability: a tendency of increased viability was observed for materials with a higher proportion of ALG in the composition. Nonetheless, seven days post-seeding, significant statistical differences ($p < 0.01$) were noticed for AC31 than for AC11 and a better cell response at the interface with ALG hydrogels was generated when citric acid was used as a crosslinker instead of $CaCl_2$.

Evaluation at two days post-seeding of the LMP-based samples revealed a statistically higher cell viability within PC31/ci with respect to PC11/ci ($p < 0.05$). The same statistical difference was observed for PC31/Ca^{2+} versus PC11/Ca^{2+}, demonstrating increased viability of cells in contact with the scaffolds containing more pectin. Upon seven days of cell seeding a statistical significant increase of viability ($p < 0.01$) was observed for cells when in contact with LMP-based scaffolds with equal mass ratio (LMP:CNFs = 1:1), the crosslinking with citric acid presenting better results compared with Ca^{2+} mediated crosslinking. The same observation and statistical significant difference ($p < 0.01$) was obtained for LMP rich materials. Besides, a significantly higher difference ($p < 0.001$) of viability between crosslinking with $CaCl_2$ and citric acid was observed, proving that citric acid represents an effective crosslinker to generate hydrogels with favourable biological activity. Overall, although statistical significant difference ($p < 0.01$) of proliferation was noticed employing the crosslinking with Ca^{2+}, higher proliferation ($p < 0.001$) was obtained employing the crosslinking with citric acid.

Significantly higher proliferation ($p < 0.001$) was detected when raising the ALG / LMP: CNFs ratio and when citric acid was used for crosslinking. Global results showed cells differentiated behaviour in contact with ALG- or LMP-based scaffolds, depending on the ratio used between polymers and the crosslinking method.

5.7. Materials cytotoxicity- LDH assay

The cytotoxicity of the synthesized materials was evaluated using LDH assay. An overall low cytotoxicity profile was registered both for ALG-based and for LMP-based materials (Fig. 8 a, b). In both cases, no significant differences in LDH levels were found after 2 days of culture, showing that the influence of the material's composition or crosslinker type on cell behaviour was not visible. Statistically significant differences appeared up to 7 days of culture. Both in ALG-based and LMP-based materials, increasing the hydrocolloid content reduces the cytotoxicity significantly ($p < 0.05$). In addition, it can be noticed that the crosslinking system determines differences in cytotoxicity levels, citric acid-crosslinked samples being more cell-friendly when compared to calcium regardless of the hydrocolloid amount.

5.8. Live/dead assay

Qualitative analysis of live and dead cells, as well as cell distribution in the 3D biomaterials was achieved using Live/Dead assay and visualization by confocal microscopy (Fig. 9 a, b). Following the Live/Dead assay staining, a good cell viability rate was observed on all types of compositions, due to the natural compounds in materials' structure. However, an increased cell viability and a better cell proliferation were observed both on the AC31 and PC31, as compared to AC11 and PC11, respectively. Also, cell viability, proliferation, morphology and grouping were the highest on LMP-rich hydrogels. An increased cell density on LMP-based scaffolds was found after 7 days of culture in standard conditions compared to ALG-containing samples. This suggests that LMP addition induced a better cellular response of hASCs in contrast to ALG.

5.9. Cytoskeleton development

The cytoskeleton consists of three units, respectively actin filaments, intermediate filaments and microtubules, which play important functions in cell morphology, adhesion, cell growth or cell signalling. Actin filaments are polar and their polymerization influences the mobility of eukaryotic cells and interaction of the cells with the environment.

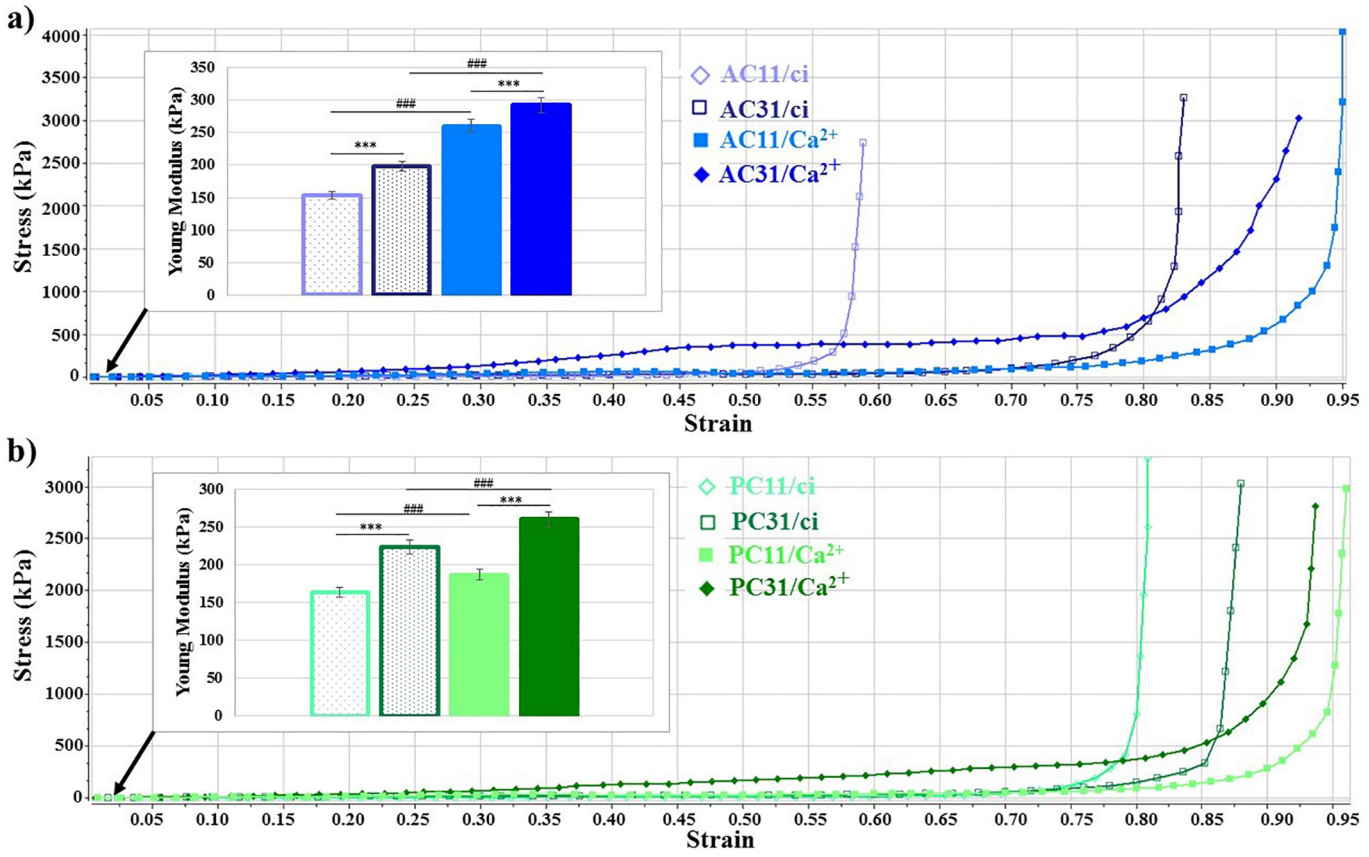

Fig. 6. The influence of crosslinking strategy upon the elastic behaviour of the synthesized hydrogels: stress-strain profiles of ALG-based hydrogels (a) and LMP-based hydrogels (b); Young's modulus values calculated at 2% strain in the corresponding inset:: $^{***}p < 0.001$(AC11/ci versus AC31/ci, AC11/ Ca^{2+} versus AC31/Ca^{2+}, PC11/ci versus PC31/ci, PC11/ Ca^{2+} versus PC31/Ca^{2+}), ###p < 0.001(AC11/ci versus AC11/Ca^{2+}, AC31/ci versus AC31/Ca^{2+},PC11/ci versus PC11/Ca^{2+},PC31/ci versus PC31/Ca^{2+}).

F-actin filaments staining (Fig. 10) revealed differences in cell behaviour in terms of adhesion to the LMP or ALG-based materials. As shown in Fig. 10, cells adhered and formed groups of cells in contact with AC materials, but cell morphology remained overall rounded, suggesting that cells adhered to the substrates, but did not develop extended cytoskeletons. Nonetheless, hASCs formed smaller groups on AC11 than on AC31, regardless the crosslinking procedure. This observation may be correlated to the higher ALG proportion within the hydrogels, which also influenced the rounded phenotype. In contrast, cells grown in contact with LMP scaffolds displayed elongated F-actin fibers both for PC11 and PC31. LMP's positive influence on cell morphology and behaviour was clearly proven, since cells were capable to form large groups and to develop long actin cytoskeleton in response to material composition. The most developed cytoskeleton was found in PC31/ci, suggesting also that citric acid crosslinking method is more efficient to generate a friendlier microenvironment than calcium-based

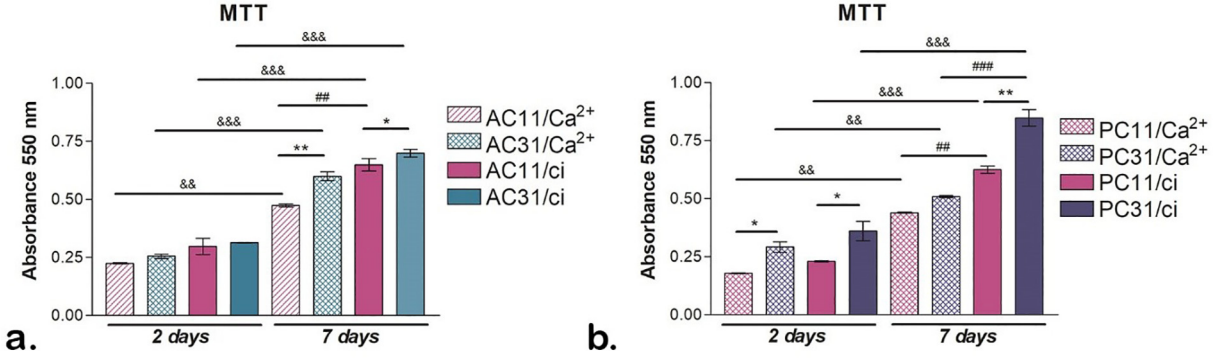

Fig. 7. Biocompatibility assessment of ALG- and LMP- containing scaffolds in contact with hASCs. [a] hASCs viability and proliferation profile evaluation after 2 and 7 days of contact with ALG-containing materials, as revealed by MTT assay: $^{**}p < 0.01$ (AC11/Ca^{2+} versus AC31/Ca^{2+} at 7 days), $^{*}p < 0.05$ (AC11/ci versus AC31/ci at 7 days), $^{\#\#}$p < 0.01 (AC11/Ca^{2+} versus AC11/ci at 7 days), $^{\&\&}$p < 0.01 (AC11/Ca^{2+} at 2 days versus AC11/Ca^{2+} at 7 days), $^{\&\&\&}p < 0.001$ (AC31/Ca^{2+} at 2 days versus AC31/ci at 7 days, AC11/ci at 2 days and AC11/ci at 7 days and AC31/ci at 2 days and AC31/ci at 7 days); [b] hASCs viability and proliferation profile evaluation after 2 and 7 days of contact with LMP-containing materials, employing MTT assay: $^{*}p < 0.05$ (PC11/Ca^{2+} versus PC31/Ca^{2+} at 2 days and PC11/ci versus PC31/ci at 2 days), $^{\#\#}p < 0.01$ (PC11/Ca^{2+} versus PC11/ci at 7 days), $^{**}p < 0.01$ (PC11/ci versus PC31/ci at 7 days), $^{\#\#\#}p < 0.001$ (PC31/Ca^{2+} versus PC31/ci at 7 days), $^{\&\&}p < 0.01$ (PC11/Ca^{2+} at 2 days versus PC11/Ca^{2+} at 7 days and PC31/Ca^{2+} at 2 days versus PC31/Ca^{2+} at 7 days), $^{\&\&\&}p < 0.001$ (PC11/ci at 2 days versus PC11/ci at 7 days and PC31/ci at 2 days and PC31/ci at 7 days).

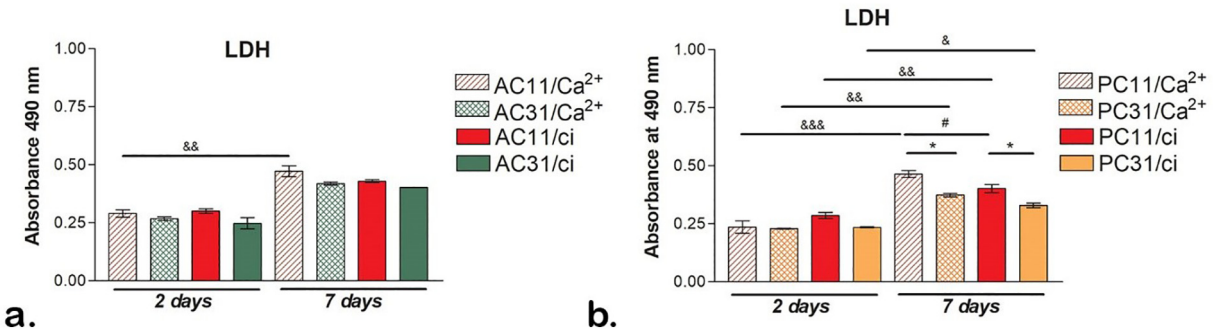

Fig. 8. ALG- and LMP- containing scaffolds cytotoxicity evaluation in contact with hASCs. [a] ALG-based materials cytotoxicity profile evaluation employing LDH assay after 2 and 7 days of cells culture: $^{**}p < 0.01$ ($AC11/Ca^{2+}$ versus $AC31/Ca^{2+}$ at 7 days), $^{*}p < 0.05$ (AC11/ci versus AC31/ci at 7 days), $^{\#\#}p < 0.01$ ($AC11/Ca^{2+}$ versus AC11/ci at 7 days), $^{\&\&}p < 0.01$ ($AC11/Ca^{2+}$ at 2 days versus $AC11/Ca^{2+}$ at 7 days), $^{\&\&\&}p < 0.001$ ($AC31/Ca^{2+}$ at 2 days versus $AC31/Ca^{2+}$ at 7 days and AC11/ci at 2 days versus AC11/ci at 7 days and AC31/ci at 2 days versus AC31/ci at 7 days); [b] LMP-based materials cytotoxicity profile evaluation by LDH assay after 2 and 7 days of cells culture: $^{*}p < 0.05$ ($PC11/Ca^{2+}$ versus $PC31/Ca^{2+}$ at 7 days and PC11/ci versus PC31/ci at 7 days), $^{\#}p < 0.05$ ($PC11/Ca^{2+}$ versus PC11/ci at 7 days), $^{\&\&\&}p < 0.001$ ($PC11/Ca^{2+}$ at 2 days versus $PC11/Ca^{2+}$ at 7 days), $^{\&\&}p < 0.01$ ($PC31/Ca^{2+}$ at 2 days versus $PC31/Ca^{2+}$ at 7 days and PC11/ci at 2 days versus PC11/ci acid at 7 days), $^{\&}p < 0.05$ (PC31/ci at 2 days versus PC31/ci at 7 days).

crosslinking. Therefore, taking into consideration its efficiency and biocompatibility, the citric acid crosslinking could generate completely bio-based polymer networks. We envisage that the new crosslinking strategy could be beneficial for supporting enhanced cellular activity.

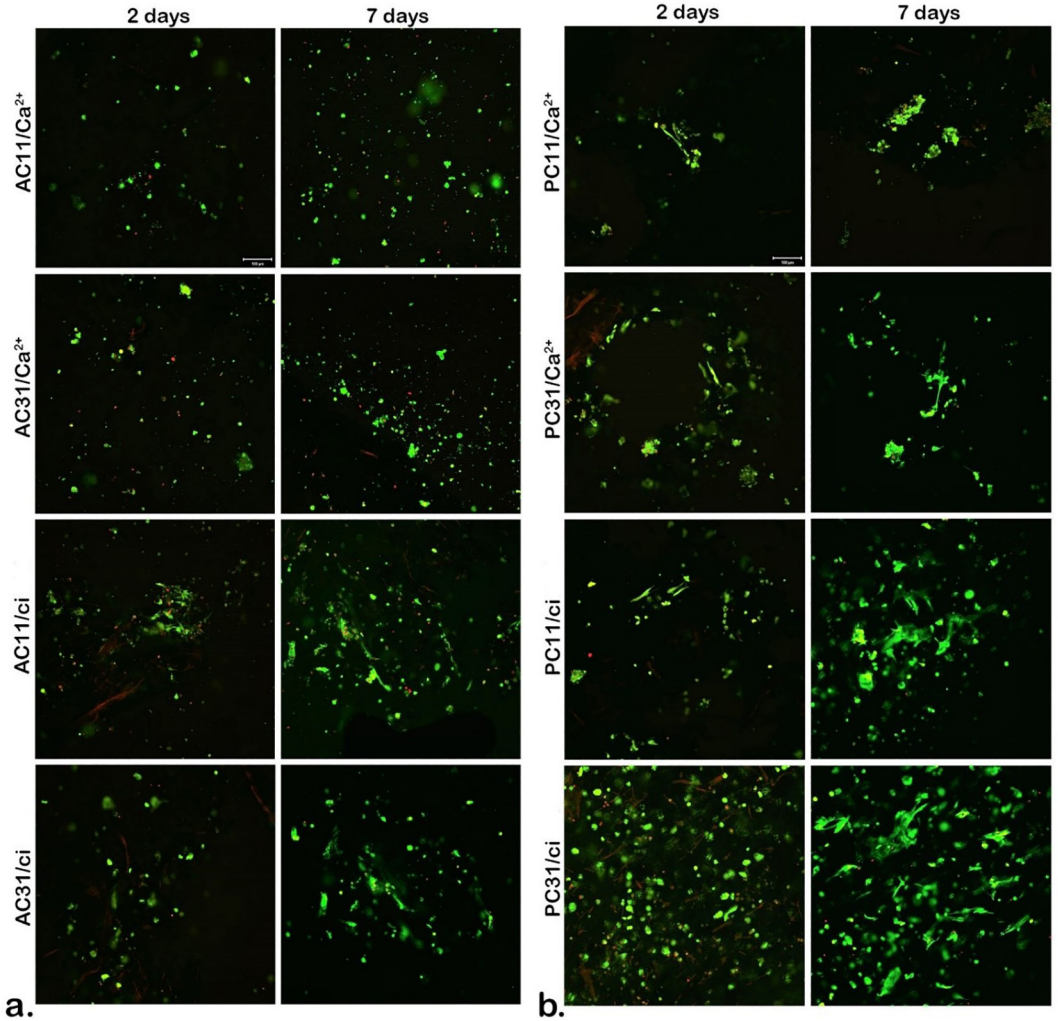

Fig. 9. Qualitative evaluation of cell viability and proliferation profile during 7 days of culture visualized by LiveDead staining and confocal microscopy in (a) ALG-based materials and (b) LMP-based materials. Live cells are stained in green. Dead cells nuclei are stained in red.

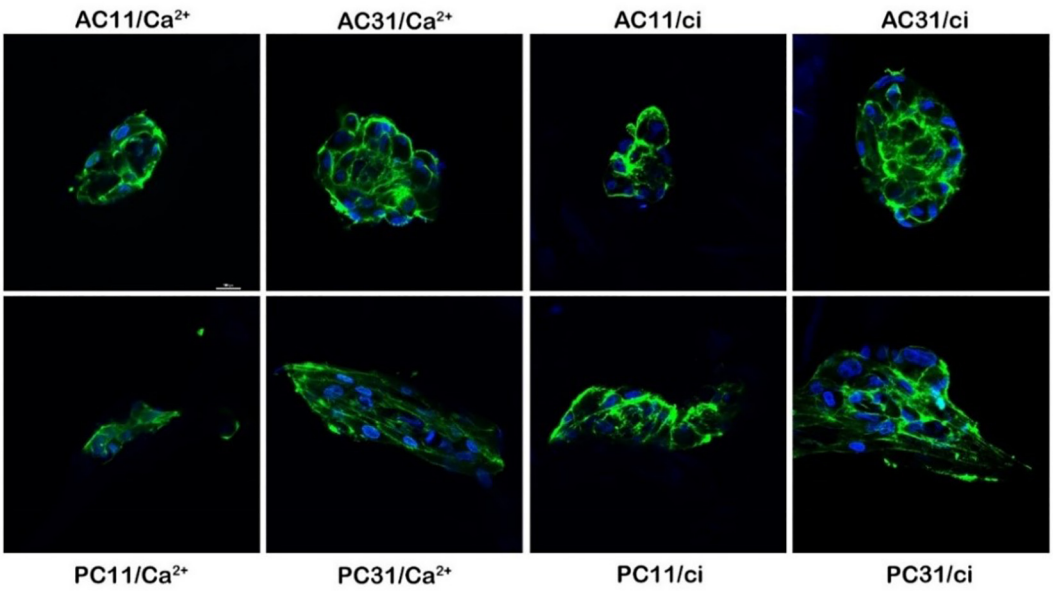

Fig. 10. F-actin filaments (green) developed by hASCs in contact with ALG- and LMP-containing scaffolds during 48 h of culture, as revealed by phalloidin-FITC staining and confocal microscopy. Cell nuclei are stained in blue.

6. Conclusions

Since the development of feasible hydrogel formulations based on physical bonds via a facile approach is still elusive, the present study provided a novel strategy to design polysaccharide-based hydrogels using a natural hydrocolloid along with nanocellulose fibrils, by exploiting citric acid capability of bridging chains with similar chemical structures. Therefore, animal origin free tailored materials can be obtained using nature as source of inspiration and thus entirely relying on plant sources. It is reasonable to assume that intermolecular H bonds with water molecules tends to break in the presence of citric acid in favor of intermolecular H bonds between polymeric chains. The formation of new crosslinks is favored since hydroxyl and carbonyl groups are present in the structure of both the polymers and citric acid. Hence it seems that particularly, these polysaccharide chain entanglements lead to supramolecular assemblies in the form of physical crosslinked gels.

Through such intermolecular interactions that are likely to associate, a complex 3D network can be generated leading to material properties tailorable for specific biomedical applications. This study showed that acid-induced gelation provides 3D highly porous networks (with nanocellulose entanglements within hydrocolloidal matrices) that exhibit better structural and functional resemblance with native (living) tissue in comparison to classical ionotropic hydrogels. All materials have shown to be biocompatible, and yet the best cellular response was obtained using hydrogels crosslinked with citric acid taking into account that the diffusion of Ca^{2+} ions out into physiological environment is held responsible for an inflammatory response [67]. Moreover, with a higher hydrocolloid content, an enhanced cellular response is generated and compulsory properties sought in regenerative medicine might be reached.

The proposed facile strategy of achieving hydrogels can be adapted for other acidic polysaccharides broadening the employment of biopolymers as scaffolding substances for the obtaining of novel hydrogels consisting of natural ingredients.

Declaration of Competing Interest

None.

Acknowledgement

The authors would like to thank for the financial support provided by a grant of the Romanian Ministery of Research and Innovation, CCCDI – UEFISCDI, project number PN-III-P1-1.2-PCCDI-2017-0782 / REGMED – project 4 TUMOR, within PNCDI III. Parts of this work was supported by a grant of the Romanian Ministry of Education and Research, CNCS - UEFISCDI, project number PN-III-P1-1.1-TE-2019-0787, within PNCDI III. Parts of this work has also been funded by the Research Council of Norway through the NORCEL project (Grant no. 228147).

References

[1] D. Howard, L.D. Buttery, K.M. Shakesheff, S.J. Roberts, Tissue engineering: strategies, stem cells and scaffolds, J. Anat. 213 (1) (2008) 66–72, https://doi.org/10.1111/j.1469-7580.2008.00878.x.
[2] C.T. Gomillion, K.J. Burg, Stem cells and adipose tissue engineering, Biomaterials. 27 (36) (2006) 6052–6063, https://doi.org/10.1016/j.biomaterials.2006.07.033.
[3] K. Lee, J. Hong, H.J. Roh, S.H. Kim, H. Lee, S.K. Lee, C. Cha, Dual ionic crosslinked interpenetrating network of alginate-cellulose beads with enhanced mechanical properties for biocompatible encapsulation, Cellulose. 24 (11) (2017) 4963–4979, https://doi.org/10.1007/s10570-017-1458-8.
[4] B.Y. Swamy, J.H. Chang, H. Ahn, W.-K. Lee, I. Chung, Thermoresponsive N-vinyl caprolactam grafted sodium alginate hydrogel beads for the controlled release of an anticancer drug, Cellulose. 20 (3) (2013) 1261–1273, https://doi.org/10.1007/s10570-013-9897-3.
[5] M. Ashford, J. Fell, D. Attwood, H. Sharma, P. Woodhead, An evaluation of pectin as a carrier for drug targeting to the colon, J. Control. Release 26 (3) (1993) 213–220, https://doi.org/10.1016/0168-3659(93)90188-B.
[6] K. Butte, M. Momin, H. Deshmukh, Optimisation and in vivo evaluation of pectin based drug delivery system containing Curcumin for Colon, Int. J. Biomater. 2014 (2014) 924278, https://doi.org/10.1155/2014/924278.
[7] V.V. Glinsky, A. Raz, Modified citrus pectin anti-metastatic properties: one bullet, multiple targets, Carbohydr. Res. 344 (14) (2009) 1788–1791, https://doi.org/10.1016/j.carres.2008.08.038.
[8] M. Farokhi, F. Jonidi Shariatzadeh, A. Solouk, H. Mirzadeh, Alginate based scaffolds for cartilage tissue engineering: a review, J. Polym. Mater. Po. (2019) 1–18, https://doi.org/10.1080/00914037.2018.1562924.
[9] J. Venkatesan, I. Bhatnagar, P. Manivasagan, K.-H. Kang, S.-K. Kim, Alginate composites for bone tissue engineering: a review, Int. J. Biol. Macromol. 72 (2015) 269–281, https://doi.org/10.1016/j.ijbiomac.2014.07.008.
[10] M. Tummalapalli, M. Berthet, B. Verrier, B.L. Deopura, M.S. Alam, B. Gupta, Composite wound dressings of pectin and gelatin with aloe vera and curcumin as bioactive

agents, Int. J. Biol. Macromol. 82 (2016) 104–113, https://doi.org/10.1016/j.ijbiomac.2015.10.087.
[11] I.A. Brownlee, A. Allen, J.P. Pearson, P.W. Dettmar, M.E. Havler, M.R. Atherton, E. Onsøyen, Alginate as a source of dietary Fiber, Crit. Rev. Food Sci. Nutr. 45 (6) (2005) 497–510, https://doi.org/10.1080/10408390500285673.
[12] S. Šešlija, A. Nešić, J. Ružić, M. Kalagasidis Krušić, S. Veličković, R. Avolio, G. Santagata, M. Malinconico, Edible blend films of pectin and poly(ethylene glycol): preparation and physico-chemical evaluation, Food Hydrocoll. 77 (2018) 494–501, https://doi.org/10.1016/j.foodhyd.2017.10.027.
[13] H. Jahangirian, E.G. Lemraski, R. Rafiee-Moghaddam, T.J. Webster, A review of using green chemistry methods for biomaterials in tissue engineering, Int. J. Nanomedicine 13 (2018) 5953–5969, https://doi.org/10.2147/IJN.S163399.
[14] N. Halib, F. Perrone, M. Cemazar, B. Dapas, R. Farra, M. Abrami, G. Chiarappa, G. Forte, F. Zanconati, G. Pozzato, L. Murena, N. Fiotti, R. Lapasin, L. Cansolino, G. Grassi, M. Grassi, Potential applications of nanocellulose-containing materials in the biomedical field, Materials (Basel) 10 (8) (2017) 977, https://doi.org/10.3390/ma10080977.
[15] M. Jorfi, E.J. Foster, Recent advances in nanocellulose for biomedical applications, J. Appl. 132 (14) (2015)https://doi.org/10.1002/app.41719.
[16] R. Curvello, V.S. Raghuwanshi, G. Garnier, Engineering nanocellulose hydrogels for biomedical applications, J. Colloid. 267 (2019) 47–61, https://doi.org/10.1016/j.cis.2019.03.002.
[17] J. Bhandari, H. Mishra, P.K. Mishra, R. Wimmer, F.J. Ahmad, S. Talegaonkar, Cellulose nanofiber aerogel as a promising biomaterial for customized oral drug delivery, Int. J. Nanomedicine 12 (2017) 2021–2031, https://doi.org/10.2147/IJN.S124318.
[18] A.B. Meneguin, B.S. Ferreira Cury, A.M. dos Santos, D.F. Franco, H.S. Barud, E.C. da Silva Filho, Resistant starch/pectin free-standing films reinforced with nanocellulose intended for colonic methotrexate release, Carbohydr. Polym. 157 (2017) 1013–1023, https://doi.org/10.1016/j.carbpol.2016.10.062.
[19] P. Gupta, B. Singh, A.K. Agrawal, P.K. Maji, Low density and high strength nanofibrillated cellulose aerogel for thermal insulation application, Mater. Des. 158 (2018) 224–236, https://doi.org/10.1016/j.matdes.2018.08.031.
[20] B. Uribe, E. Chiromito, A. Carvalho, R. Arenal, J. Tarpani, TEMPO-oxidized cellulose nanofibers as interfacial strengthener in continuous-fiber reinforced polymer composites, Mater. Des. 133 (2017) 340–348, https://doi.org/10.1016/j.matdes.2017.08.004.
[21] K. Ganesan, A. Dennstedt, A. Barowski, L. Ratke, Design of aerogels, cryogels and xerogels of cellulose with hierarchical porous structures, Mater. Des. 92 (2016) 345–355, https://doi.org/10.1016/j.matdes.2015.12.041.
[22] M.C. Mulakkal, R.S. Trask, V.P. Ting, A.M. Seddon, Responsive cellulose-hydrogel composite ink for 4D printing, Mater. Des. 160 (2018) 108–118, https://doi.org/10.1016/j.matdes.2018.09.009.
[23] M.J. Costa, A.M. Marques, L.M. Pastrana, J.A. Teixeira, S.M. Sillankorva, M.A. Cerqueira, Physicochemical properties of alginate-based films: effect of ionic crosslinking and mannuronic and guluronic acid ratio, Food Hydrocoll. 81 (2018) 442–448, https://doi.org/10.1016/j.foodhyd.2018.03.014.
[24] K.Y. Lee, D.J. Mooney, Alginate: properties and biomedical applications, Prog. Polym. Sci. 37 (1) (2012) 106–126, https://doi.org/10.1016/j.progpolymsci.2011.06.003.
[25] G. Tripathi, J. Gwon, S.-Y. Lee, B.-T. Lee, Novel TOCNF reinforced injectable alginate/β-tricalcium phosphate microspheres for bone regeneration, Mater. Des. 108892 (2020)https://doi.org/10.1016/j.matdes.2020.108892.
[26] M. Mihai, C. Steinbach, M. Aflori, S. Schwarz, Design of high sorbent pectin/CaCO3 composites tuned by pectin characteristics and carbonate source, Mater. Des. 86 (2015) 388–396, https://doi.org/10.1016/j.matdes.2015.07.088.
[27] M.D. Walkinshaw, S. Arnott, Conformations and interactions of pectins: II. Models for junction zones in pectinic acid and calcium pectate gels, J. Mol. Biol. 153 (4) (1981) 1075–1085, https://doi.org/10.1016/0022-2836(81)90468-X.
[28] M. Watase, K. Nishinari, Effects of pH and DMSO content on the thermal and rheological properties of high methoxyl pectin-water gels, Carbohydr. Polym. 20 (3) (1993) 175–181, https://doi.org/10.1016/0144-8617(93)90148-W.
[29] H. Kastner, U. Einhorn-Stoll, B. Senge, Structure formation in sugar containing pectin gels – influence of Ca2+ on the gelation of low-methoxylated pectin at acidic pH, Food Hydrocoll. 27 (1) (2012) 42–49, https://doi.org/10.1016/j.foodhyd.2011.09.001.
[30] D.E. Ngouémazong, F.F. Tengweh, I. Fraeye, T. Duvetter, R. Cardinaels, A. Van Loey, P. Moldenaers, M. Hendrickx, Effect of de-methylesterification on network development and nature of Ca2+−pectin gels: towards understanding structure–function relations of pectin, Food Hydrocoll. 26 (1) (2012) 89–98, https://doi.org/10.1016/j.foodhyd.2011.04.002.
[31] A. Ström, P. Ribelles, L. Lundin, I. Norton, E.R. Morris, M.A.K. Williams, Influence of pectin fine structure on the mechanical properties of calcium−pectin and acid−pectin gels, Biomacromolecules. 8 (9) (2007) 2668–2674, https://doi.org/10.1021/bm070192r.
[32] S. Groult, T. Budtova, Tuning structure and properties of pectin aerogels, Eur. Polym. J. 108 (2018) 250–261, https://doi.org/10.1016/j.eurpolymj.2018.08.048.
[33] M.M. Pérez-Madrigal, J. Torras, J. Casanovas, M. Häring, C. Alemán, D.D. Díaz, Paradigm shift for preparing versatile M2+-free gels from unmodified sodium alginate, Biomacromolecules. 18 (9) (2017) 2967–2979, https://doi.org/10.1021/acs.biomac.7b00934.
[34] K.I. Draget, G. Skjåk Bræk, O. Smidsrød, Alginic acid gels: the effect of alginate chemical composition and molecular weight, Carbohydr. Polym. 25 (1) (1994) 31–38, https://doi.org/10.1016/0144-8617(94)90159-7.
[35] K.I. Draget, G. Skjåk-Bræk, B.E. Christensen, O. Gåserød, O. Smidsrød, Swelling and partial solubilization of alginic acid gel beads in acidic buffer, Carbohydr. Polym. 29 (3) (1996) 209–215, https://doi.org/10.1016/0144-8617(96)00029-X.
[36] K.I. Draget, B.T. Stokke, Y. Yuguchi, H. Urakawa, K. Kajiwara, Small-angle X-ray scattering and rheological characterization of alginate gels. 3. Alginic acid gels, Biomacromolecules 4 (6) (2003) 1661–1668, https://doi.org/10.1021/bm034105g.
[37] C. Demitri, R. Del Sole, F. Scalera, A. Sannino, G. Vasapollo, A. Maffezzoli, L. Ambrosio, L. Nicolais, Novel superabsorbent cellulose-based hydrogels crosslinked with citric acid, J. Appl. 110 (4) (2008) 2453–2460, https://doi.org/10.1002/app.28660.
[38] M.G. Raucci, M.A. Alvarez-Perez, C. Demitri, D. Giugliano, V. De Benedictis, A. Sannino, L. Ambrosio, Effect of citric acid crosslinking cellulose-based hydrogels on osteogenic differentiation, J. Biomed. Mater. Res. A 103 (6) (2015) 2045–2056, https://doi.org/10.1002/jbm.a.35343.
[39] K. Mali, S.C. Dhawale, R. Dias, N. Dhane, V. Ghorpade, Citric acid crosslinked carboxymethyl cellulose-based composite hydrogel films for drug delivery, Indian J. Pharm. Sci. 80 (2018) 657–667, https://doi.org/10.4172/pharmaceutical-sciences.1000405.
[40] H. Fahmy, M.M. Fouda, Crosslinking of alginic acid/chitosan matrices using polycarboxylic acids and their utilization for sodium diclofenac release, Carbohydr. Polym. 73 (4) (2008) 606–611, https://doi.org/10.1016/j.carbpol.2007.12.024.
[41] R. Lusiana, D. Siswanta, M. Mudasir, Preparation of citric acid crosslinked chitosan/poly(Vinyl alcohol) blend membranes for creatinine transport, Indones. J. Chem. 16 (2016) 144–150, https://doi.org/10.14499/ijc-v16i2p144-150.
[42] S.A. Stone, P. Gosavi, T.J. Athauda, R.R. Ozer, In situ citric acid crosslinking of alginate/polyvinyl alcohol electrospun nanofibers, Mater. Lett. 112 (2013) 32–35, https://doi.org/10.1016/j.matlet.2013.08.100.
[43] P. Singh, P. Baisthakur, O.S. Yemul, Synthesis, characterization and application of crosslinked alginate as green packaging material, Heliyon 6 (1) (2020), e03026, https://doi.org/10.1016/j.heliyon.2019.e03026.
[44] S. Ye, Z. Zhu, Y. Wen, C. Su, L. Jiang, S. He, W. Shao, Facile and green preparation of pectin/cellulose composite films with enhanced antibacterial and antioxidant behaviors, Polymers. 11 (2019) 57, https://doi.org/10.3390/polym11010057.
[45] W.J. Zheng, J. Gao, Z. Wei, J. Zhou, Y.M. Chen, Facile fabrication of self-healing carboxymethyl cellulose hydrogels, Eur. Polym. J. 72 (2015) 514–522, https://doi.org/10.1016/j.eurpolymj.2015.06.013.
[46] T. Saito, Y. Nishiyama, J.-L. Putaux, M. Vignon, A. Isogai, Homogeneous suspensions of individualized microfibrils from TEMPO-catalyzed oxidation of native cellulose, Biomacromolecules. 7 (6) (2006) 1687–1691, https://doi.org/10.1021/bm060154s.
[47] A.I. Cernencu, A. Lungu, I.-C. Stancu, A. Serafim, E. Heggset, K. Syverud, H. Iovu, Bioinspired 3D printable pectin-nanocellulose ink formulations, Carbohydr. Polym. 220 (2019) 12–21, https://doi.org/10.1016/j.carbpol.2019.05.026.
[48] G. Manrique, F. Lajolo, FT-IR spectroscopy as a tool for measuring degree of methyl esterification in pectins isolated from ripening papaya fruit, Postharvest Biol Tec. 25 (2002) 99–107, https://doi.org/10.1016/S0925-5214(01)00160-0.
[49] C. Kyomugasho, S. Christiaens, A. Shpigelman, A.M. Van Loey, M.E. Hendrickx, FT-IR spectroscopy, a reliable method for routine analysis of the degree of methylesterification of pectin in different fruit- and vegetable-based matrices, Food Chem. 176 (2015) 82–90, https://doi.org/10.1016/j.foodchem.2014.12.033.
[50] M. Szymanska-Chargot, A. Zdunek, Use of FT-IR spectra and PCA to the bulk characterization of Cell Wall residues of fruits and vegetables along a fraction process, Food Biophys. 8 (1) (2013) 29–42, https://doi.org/10.1007/s11483-012-9279-7.
[51] S. Gulrez, S. Al-Assaf, G. Phillips, Hydrogels: methods of preparation, characterisation and applications, in: A. Carpi (Ed.), Progress in Molecular and Environmental Bioengineering-from Analysis and Modeling to technology applications, InTechOpen 2011, p. 660.
[52] C.K. Kuo, P.X. Ma, Ionically crosslinked alginate hydrogels as scaffolds for tissue engineering: Part 1. Structure, gelation rate and mechanical properties, Biomaterials 22 (6) (2001) 511–521, https://doi.org/10.1016/S0142-9612(00)00201-5.
[53] F. Munarin, S.G. Guerreiro, M.A. Grellier, M.C. Tanzi, M.A. Barbosa, P. Petrini, P.L. Granja, Pectin-based injectable biomaterials for bone tissue engineering, Biomacromolecules. 12 (3) (2011) 568–577, https://doi.org/10.1021/bm101110x.
[54] A.A. Jack, H.R. Nordli, L.C. Powell, D.J.J. Farnell, B. Pukstad, P.D. Rye, D.W. Thomas, G. Chinga-Carrasco, K.E. Hill, Cellulose Nanofibril formulations incorporating a low-molecular-weight alginate oligosaccharide modify bacterial biofilm development, Biomacromolecules 20 (8) (2019) 2953–2961, https://doi.org/10.1021/acs.biomac.9b00522.
[55] O. Aarstad, E.B. Heggset, I. Pedersen, S. Bjørnøy, K. Syverud, B. Strand, Mechanical properties of composite hydrogels of alginate and cellulose Nanofibrils, Polymers. 9 (2017) 378, https://doi.org/10.3390/polym9080378.
[56] M. Takigami, H. Amada, N. Nagasawa, T. Yagi, T. Kasahara, S. Takigami, M. Tamada, Preparation and properties of CMC gel, Trans. Mater. Res. Soc. Jpn. 32 (2007) 713–716.
[57] M. Wang, L. Xu, X. Ju, J. Peng, M. Zhai, J. Li, G. Wei, Enhanced radiation crosslinking of carboxymethylated chitosan in the presence of acids or polyfunctional monomers, Polym. Degrad. 93 (10) (2008) 1807–1813, https://doi.org/10.1016/j.polymdegradstab. 2008.07.013.
[58] C. Sandeep, S. Harikumar, Hydrogels: a smart drug delivery system, Int. J. Res. Pharm. Chem. 2 (3) (2012) 603–614http://www.ijrpc.com/files/08-294.pdf.
[59] P. Siqueira, É. Siqueira, A.E. de Lima, G. Siqueira, A.D. Pinzón-Garcia, A.P. Lopes, M.E.C. Segura, A. Isaac, F.V. Pereira, V.R. Botaro, Three-dimensional stable alginate-nanocellulose gels for biomedical applications: towards tunable mechanical properties and cell growing, Nanomaterials (Basel) 9 (1) (2019) 78, https://doi.org/10.3390/nano9010078.
[60] S. Fujisawa, Y. Okita, H. Fukuzumi, T. Saito, A. Isogai, Preparation and characterization of TEMPO-oxidized cellulose nanofibril films with free carboxyl groups, Carbohydr. Polym. 84 (1) (2011) 579–583, https://doi.org/10.1016/j.carbpol.2010.12.029.

[61] C. Sartori, D.S. Finch, B. Ralph, K. Gilding, Determination of the cation content of alginate thin films by FTi.r. spectroscopy, Polymer 38 (1) (1997) 43–51, https://doi.org/10.1016/S0032-3861(96)00458-2.
[62] H. Daemi, M. Barikani, Synthesis and characterization of calcium alginate nanoparticles, sodium homopolymannuronate salt and its calcium nanoparticles, SCI IRAN. 19 (6) (2012) 2023–2028, https://doi.org/10.1016/j.scient.2012.10.005.
[63] B. Murray, Inhibition of ice crystallisation in highly viscous aqueous organic acid droplets, Atmos. Chem. Phys. 8 (2008)https://doi.org/10.5194/acpd-8-8743-2008.
[64] A. Bogdan, M.J. Molina, H. Tenhu, T. Loerting, Multiple glass transitions and freezing events of aqueous citric acid, J. Phys. Chem. A 119 (19) (2015) 4515–4523, https://doi.org/10.1021/jp510331h.
[65] N.F.A.-Z. Tuan Mohamood, N. Zainuddin, M. Ahmad, S.W. Tan, Preparation, optimization and swelling study of carboxymethyl sago starch (CMSS)–acid hydrogel, Chem. Cent. J. 12 (1) (2018) 133, https://doi.org/10.1186/s13065-018-0500-8.
[66] S.K. Bajpai, S. Sharma, Investigation of swelling/degradation behaviour of alginate beads crosslinked with Ca2+ and Ba2+ ions, React. Funct. Polym. 59 (2) (2004) 129–140, https://doi.org/10.1016/j.reactfunctpolym.2004.01.002.
[67] G. Chan, D.J. Mooney, Ca(2+) released from calcium alginate gels can promote inflammatory responses in vitro and in vivo, Acta Biomater. 9 (12) (2013) 9281–9291, https://doi.org/10.1016/j.actbio.2013.08.002.